Electrowetting-assisted droplet coalescence and roll-off for condensation heat transfer enhancement

Enakshi D. Wikramanayake, Vaibhav Bahadur*

Walker Department of Mechanical Engineering, The University of Texas at Austin, Austin, TX 78712

ABSTRACT

Dropwise condensation heat transfer is significantly higher than filmwise condensation heat transfer due to the absence of the thermal resistance associated with the condensed water film. This study uses electrowetting to enhance coalescence and roll-off of condensed droplets, with the objective of enhancing the condensation rate. Coalescence enhancement is achieved by electric field-driven droplet motion such as translation of droplets, and oscillations of the three-phase line. Experiments are conducted to study early-stage droplet growth dynamics, and steady state condensation under electrowetting fields. Results show that droplet growth and roll-off increases with the voltage and frequency of the applied AC field. AC electric fields are seen to be more effective than DC electric fields. The overall condensation rate depends on the roll-off size of droplets, frequency of roll-off events, and on the interactions of the rolled-off droplets with the remainder of the droplets. All these phenomena can be altered by the applied electric field. An analytical heat transfer model is developed which uses the measured droplet size distribution to estimate the surface heat flux. Overall, this study reports that electric fields can enhance the condensation rate by more than 30 %.

Keywords: condensation, electrowetting, heat transfer, droplets.

NOMENCLATURE

a = half width of electrode gap

C = capacitance per unit area

k = dielectric constant

q = heat transfer

$R_{cond,air}$ = conduction resistance through air

$R_{cond,drop}$ = conduction resistance through the droplet

R_{diff} = diffusion resistance

R_{int} = interface resistance

$R_{Total}(r)$ = overall resistance through droplet

r = droplet radius

$< R >$ = area average radius

ΔT = temperature difference between surface and ambient

V = voltage

w = electrode width

ε_0 = permittivity of vacuum

σ = electrical conductivity

ω = angular frequency

γ = liquid-vapour surface tension

θ_{eq} = equilibrium contact angle

INTRODUCTION

Condensation of water is key to the performance of many engineering applications [1-3]. Condensation heat transfer (and rate) is limited [4] by the condensate film forming on the typically hydrophilic surface. Heat transfer can be significantly enhanced if hydrophobic surfaces are used to condense water as droplets which then roll-off [5], thereby exposing the surface to fresh vapour for re-nucleation. Dropwise condensation heat transfer coefficients are 5-10 time higher [4] as compared to filmwise condensation.

Dropwise condensation has been extensively studied [4–6] with the aim of developing surface textures and chemistry [6–9] that induce condensation as droplets. Importantly, most experimental studies on DWC involve condensation of steam or saturated vapour; there are far fewer studies on condensation in the presence of non-condensable gases [10].

In the realm of modelling, recent theoretical studies [5,11,12] have used measured droplet size distributions to estimate heat transfer using thermal resistance models.

The use of active methods (such as applying an electric field) to promote condensation heat transfer has generated significant recent interest [13,14]. This work is a study of the influence of electrowetting (EW) on coalescence, growth and roll-off dynamics of condensing droplets. EW is a well-understood [15,16] technique to control the wettability of droplets and enable various microfluidic droplet-based operations. EW is based on the application of an electrical potential across a dielectric layer underlying the droplet (electrically conducting) to modulate wettability and actuate the droplet. The Young-Lippman's equation [15,16] predicts the voltage-dependent contact angle as:

$$cos\,\theta = cos\theta_{eq} + \frac{C}{2\gamma}V^2 \qquad (1)$$

Here θ_{eq} is the equilibrium contact angle with no voltage applied and V is the applied voltage. In the experiments conducted in this study (Figure 1), the actuation electrodes have a co-planar geometry with the parallel positive and ground electrodes being separated by a non-conducting gap. In such a configuration, the field lines form an arc from the high voltage electrode to the ground [14,17]. Based on this geometry the capacitance per unit area of the dielectric layer, C, can be analytically modelled as $C = \frac{2\varepsilon_0\varepsilon_d l}{\pi A}\ln\left[\left(1 + \frac{w}{a}\right) + \sqrt{\left(1 + \frac{w}{a}\right)^2 - 1}\right]$ [18]. It is noted that the dielectric material is a critical component of EW systems. Specific requirements include high dielectric constant, high electrical breakdown field, and low surface energy.

The influence of the frequency of the AC waveform used for EW has been studied before and the understanding of its influence on condensation droplet dynamics is a key aspect of this work. The influence of AC frequency is captured by the expression for complex permittivity[15] of the droplet, $\varepsilon^* = k\varepsilon_0 - j\frac{\sigma}{\omega}$. The two terms represent the capacitance and the resistance respectively. For DC and low frequency AC waveforms, the droplet can be considered electrically conducting (equipotential). At higher frequencies, the relative influence of the electrical conductivity is reduced and the droplet behaves increasingly as an insulator. It is noted that low frequency AC fields have been used in many EW studies, since contact angle hysteresis is lower for AC fields as compared to DC fields [15,16,19].

This work [20] is a fundamental study on EW-accelerated droplet growth dynamics and droplet roll-off. Importantly, all experiments involve condensation of humid air (with significant non-condensables) and not condensation of pure steam. The influence of the applied voltage and frequency of the AC EW field on droplet coalescence is experimentally characterized, and the underlying physical mechanisms are

discussed. The influence of EW fields on condensation dynamics is studied prior to droplet shedding, and after the onset of droplet shedding. Finally, the heat transfer enhancement due to the EW field is quantified by measuring the water condensation rate.

DETAILS OF EXPERIMENTS

All experiments in this study were conducted on a single surface with coplanar parallel activated and ground electrodes. Indium Tin Oxide (ITO) coated glass slides were used as the substrate, and an interdigitated electrode layout (Figure 1a) was fabricated via lithography and plasma etching. The two sets of electrodes were connected to the high voltage and ground ends of a signal generator and amplifier. The electrode width and gap between electrodes were 50 μm each. Figure 1b shows the cross section of the surface. A 2 μm layer of CYTOP (hydrophobic fluoropolymer) was spin coated as the EW dielectric. The condensing surface was placed on a liquid nitrogen cold plate, with the surface maintained at 2±1ºC. The setup was located in an atmospheric pressure environmental chamber maintained at 23±2ºC and 60±2.5% relative humidity.
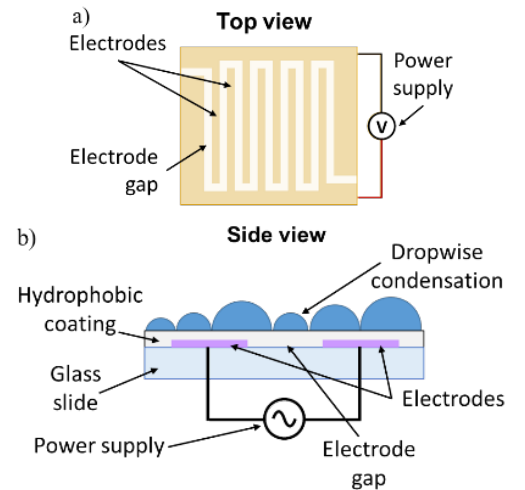

Figure 1. Schematic showing experimental setup. a) Top view showing interdigitated electrodes architecture. b) Cross section of surface [adapted from 20].

Two types of experiments were conducted. The first type involved visualization of droplet growth dynamics on horizontal surfaces (Figure 2), to analyse early-stage dynamics of droplet growth and coalescence. Condensation was started once the cold plate reached a steady 2ºC, the EW field was then turned on and remained on for the remainder of the experiments. Droplet growth was recorded with an optical microscope. Baseline experiments were conducted without any applied voltage. Next, experiments were conducted with 60 V$_{rms}$ (root mean square) and 100 V$_{rms}$ (root mean square) and at AC frequencies of 0 Hz (DC), 1 Hz and 10 kHz. No experiments were conducted above 100V to avoid breakdown of the dielectric layer. All experiments lasted 30 minutes.

For the second type of experiments, the surface was oriented vertically to enable droplet roll-off. These

2

experiments were conducted for three hours. The amount of condensed water was estimated by adding the mass of all droplets as they rolled to bottom of the condensing area. It is noted that all data in this manuscript is the average of three repetitions.

MATLAB was used for post-processing to count the number and size of condensed droplets. The imaging capabilities allowed the detection of droplets > 5 µm. Droplets were assumed to have a spherical cap geometry, with a contact angle of 120° (no EW field).

EXPERIMENTAL RESULTS

Early stage droplet growth dynamics

This section describes experimental results of condensation experiments starting from no condensate on the surface. Figure 2 shows snapshots of the surface at 10 minutes and 30 minutes for the no voltage case, 100 V_{rms}, 10 kHz case and 100 V DC case. After nucleation, droplets initially grow by condensation of vapour, and then start coalescing as they grow larger. In the absence of an EW field, droplets maintain a self-similar, as seen in Figures 2a and d.
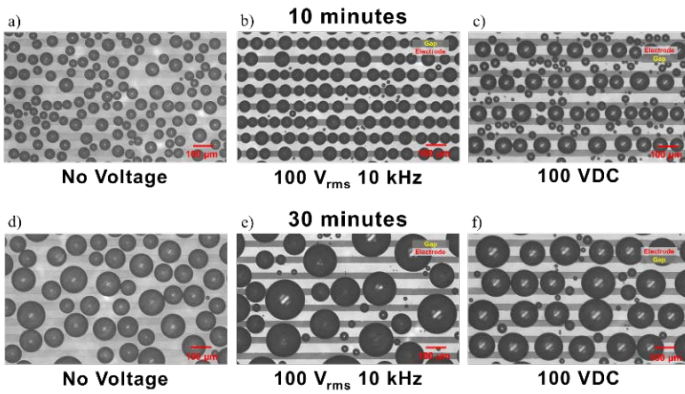

Figure 2. Droplet growth patterns under a) no voltage at 10 minutes, b) 100 Vrms, 10 kHz at 10 minutes, c) 100 VDC at 10 minutes, d) no voltage at 30 minutes, e) 100 Vrms, 10 kHz at 30 minutes, f) 100 VDC at 30 minutes [20].

These results show that an electric field alters the droplet distribution. Droplets migrate to locations where the electrostatic energy of the system is minimized; the specific location depends on the electrode and droplet geometry [15]. Droplets will migrate when the electrostatic force exceeds the friction associated with contact angle hysteresis. Also, the electric field is itself modified as the droplets grow, since droplets can be considered electrically conducting compared to the dielectric layer and air. As a result the minimum energy location can change with time [14].

Under AC fields, the minimum energy location is the centre of the gap between adjacent electrodes [14]. Accordingly, Figure 2b shows droplets aligning in the electrode gaps (dark areas). As the droplets grow, they will merge and continue to reside in the electrode gaps (Figure 2e). Another observation is the role of the AC frequency on the nature of fluid motion. At 10 kHz, droplets remain stationary,

with the three phase line oscillating in response to the AC waveform. However, at 1 Hz, in addition to the oscillatory motion of the three phase line, droplets also physically translate around their equilibrium positions. Both types of motions (oscillation, translation) enhance coalescence.

For DC fields, the droplet arrangement has a different nature as compared to AC fields. Droplets merge and then line up on the alternate electrodes. The droplets remain here and continue to grow by condensation as seen in Figure 2c and f. Under DC fields, higher contact line friction prevents them from moving continuously, unlike what is observed under AC fields. The differences between the nature of coalescence under AC and DC fields is currently being studied in more detail.
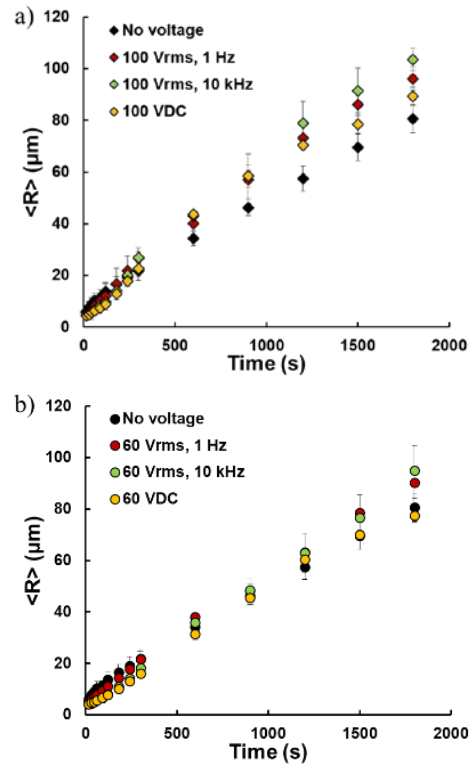

Figure 3. Timewise increase in area-weighted average radius of condensed droplets under EW voltages of a) 100 V and b) 60 V [adapted from 20].

To quantify the influence of the electric field on growth, the area-weighted average droplet radius, $<R>= \frac{\sum r^3}{\sum r^2}$ was estimated image processing. Figure 3 shows $<R>$ versus time for voltages of 100 V rms (Figure 3a) and 60 V rms (Figure 3b), with frequencies of 1 Hz, 10 kHz and 0 Hz (DC voltage), along with the baseline case. The EW electric field accelerates growth, with the differences becoming more prominent at longer times. Overall, faster growth was observed for experiments at 10 kHz, as compared to those at 1 Hz. This suggests that the reduced contact angle hysteresis associated with high frequency AC fields[14] makes it easier for droplets to move and coalesce. Interestingly, the DC field showed no noticeable improvement from the baseline. It appears that the absence of oscillatory motion of the contact line (under DC fields) reduces the capture of smaller droplets by larger ones, thereby slowing growth.
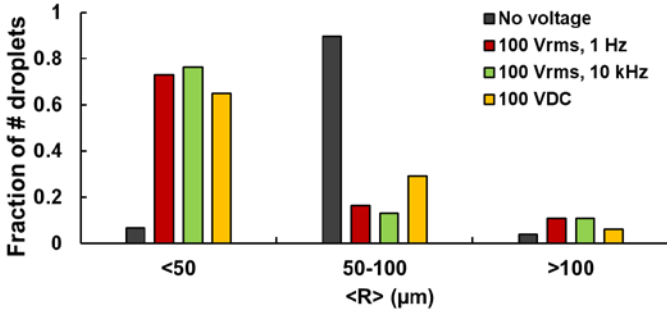
Figure 4. Size distribution of droplets condensing under the influence of electric fields after 30 minutes [adapted from 20].

Figure 4 highlights the impact of electric fields on droplet size distributions. For the baseline case, a unimodal log-normal distribution is obtained. This shows a decreasing average radius and a widening droplet size distribution with time. Under EW fields, a bi-modal or multi-modal distribution [14] is obtained, with large droplets surrounded by many small droplets. Although the distribution shows a smaller number density in the large size bin, the larger droplets account for a significant volume percentage of the total condensate. At 30 minutes, the total condensate volume in the largest bin (> 100 μm) for 100 V rms AC is 3X greater than in the baseline case.

Knowledge of droplet size distributions can be used to estimate the rate of heat transfer. Studies have used droplet size distributions in a thermal resistance model to estimate heat transfer [12]. Accordingly, the present study uses the measured droplet size distributions to estimate the heat transfer enhancement achieved via the use of EW.

Droplet roll-off and condensation rate

This section discusses experiments with vertically oriented surfaces and studied roll-off of droplets. These were longer duration experiments (three hours). Droplet roll-off occurs when the droplets reach a critical radius. Droplet mass was estimated via image processing to calculate the radius of the spherical cap shaped droplet after it rolled off.

Figure 5 shows the condensate mass flux for the baseline case, 100 Vrms 1 Hz and 100 Vrms 10 kHz. For the cases of no voltage and 100 V, 10 kHz, two distinct regions of the curve (Figure 5a) are seen. The initial, higher slope region accounts for a large number of roll-off events taking place between the times corresponding to roll-off of the first droplet, till the time that the entire area is swept at least once. The second, lower slope region corresponds to a constant condensation rate; this is referred to as steady state condensation. This is a quasi-steady process with a stable droplet size distribution. Under these conditions, classical models can be used to characterize the number density of droplets [26]. The slope of the curves in Figure 5 can be used to estimate the steady state condensation rate. The 100 V, 10 kHz case has a 33% higher condensation rate than the baseline. The 100 V, 1 Hz case has a 17% higher condensation rate than the baseline.
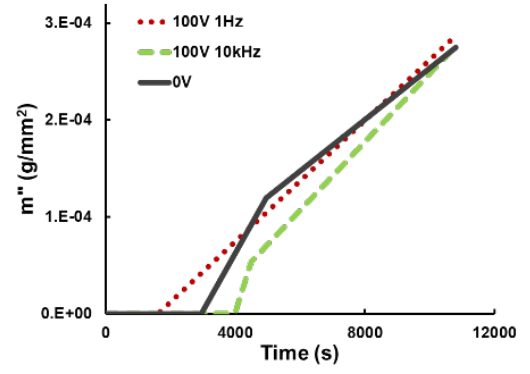

Figure 5. Condensate mass flux for three cases (no voltage, 100 V, 10 kHz, and 100 V, 1 Hz) [adapted from 20].

Figure 6a compares the roll-off radii for the three cases. Figures 6b and c compare the roll off frequency (the number of roll off events per unit area) and the time at which the first roll-off event takes place, respectively. For the no voltage case, the first roll-off event occurred at ~60 minutes and the average roll-off radius was 725±89 μm.
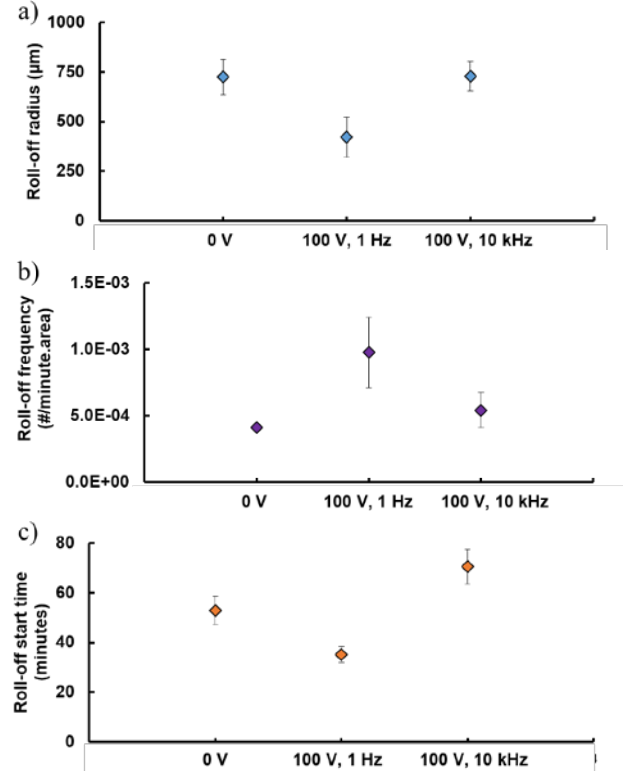

Figure 6. Key parameters associated with droplet roll-off under various cases. a) droplet roll-off radius, b) roll-off frequency, c) time of first roll-off event.

For the 100 V, 10 kHz case, the first roll-off event occurred at ~70 minutes. The average roll-off radius was 730±75 μm. This delayed roll-off is the result of the electric field pinning droplets [13], noting that the electric field lines will penetrate the droplet. The electrical pinning effect can also be inferred from the low roll-off frequency throughout the experiment. This suggests that periodically turning the electric field off will assist in droplet roll-off. Also, large droplet roll-off radii are not necessarily detrimental, as the droplet size determines the amount of condensate swept by the droplets as they roll off.

The most interesting case is the case of 100 V, 1 Hz. The first roll-off event occurred at ~30 minutes, and the average roll-off radius was 420±100 μm. This is 35% earlier and 42% less than the roll-off start time and average radius of the baseline case, respectively, as seen in Figure 6. The reason for the lower roll-off radius is the reduction in contact angle hysteresis associated with AC electric fields. Droplets are observed to oscillate around their mean position, thereby de-pinning the three-phase contact line from the surface. Additionally, the translation motion of droplets at low frequencies can lead to stochastic coalescence with other droplets, which can trigger roll-off. The high roll-off frequency can be attributed to this phenomenon. However, although the roll-off frequency is high, the average size of the rolled-off droplet is low, since the droplets have had lesser time to grow. This results in lower overall condensation rates as compared to the high frequency case. In the high frequency case, the roll-off frequency is low and the roll-off radius is the largest of all the cases studied. These large droplets capture a significant number of smaller droplets on their way down, while also opening up a large new track for fresh nucleation. Overall, these results demonstrate that condensation need not be maximized by droplets rolling-off rapidly (and at smaller sizes). Condensation also depends on the interactions of the rolling-off droplets with the rest of the droplets.

MODELING CONDENSATION HEAT TRANSFER

A thermal resistance network-based analytical model is detailed to predict condensation heat transfer rate from the knowledge of a specified droplet size distribution. In this study, the model is used to predict the heat transfer for the baseline case (no voltage). The thermal resistance network-based model extends the recent work of Zhoa et al.[10]. Since the present experiments were conducted with humid air, the thermal resistance network was modified to account for the presence of non-condensable gases. The present thermal resistance network also considers natural convection from the non-wetted area, which is an improvement over existing models which only consider heat transfer through droplets.
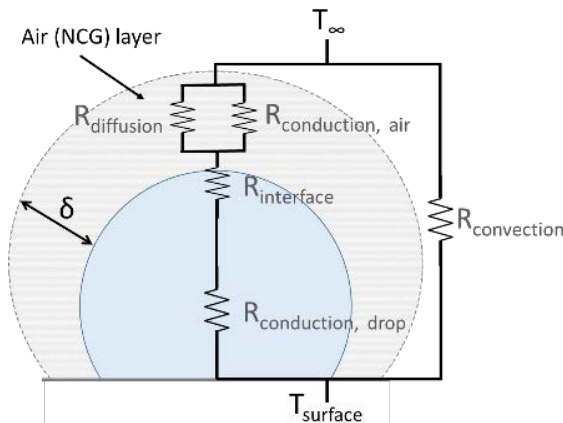

Figure 7. Thermal resistance network associated with a single droplet in dropwise condensation mode [20].

Figure 7 shows the thermal resistance network corresponding to a single droplet. It includes conduction resistance[12] through the droplet and interface resistance [4,5] at the liquid-vapour interface, with both resistances in series. Both of these terms have been used in classical models to analyse condensation heat transfer. Since this study is conducted in humid air, analysis of heat transfer in the layer of noncondensables developing around the droplet is important. Two additional resistances are therefore included in parallel, a diffusion resistance which accounts for vapour molecules diffusing through the layer of noncondensables and a conduction resistance through air in the layer of noncondensables [10]. The resulting overall thermal resistance associated with a single droplet can then be estimated as [20]:

$$R_{Total}(r) = \left[\frac{1}{R_{diff}} + \frac{1}{R_{cond,air}}\right]^{-1} + R_{int} + R_{cond,drop} \qquad (2)$$

Knowledge of the total resistance can be used to quantify the heat transfer through a single droplet as:

$$q(r) = \frac{\Delta T}{R_{Total}(r)} \qquad (3)$$

The total condensation heat flux can then be estimated by using equation 3 with the measured droplet size distribution on the surface. This model predicts a condensation heat transfer rate of 104 W/m^2 for the baseline case. While this value will seem low, it is noted that this study involved humid air condensation with significant noncondensables. Furthermore, there was no forced convection-related enhancement presently. This model will be refined and extended to predict the heat transfer enhancement benefits of electrowetting fields as part of future work.

CONCLUSIONS

Overall, this study shows that electrowetting fields can strongly influence droplet coalescence and roll-off during condensation. Important parameters which can be tuned to control condensation rates include the magnitude and frequency of the electrowetting waveform and the electrode architecture. Key findings from this study are:

- AC electrowetting fields promote greater coalescence than DC fields.
- Droplet growth rate increases with applied voltage and its frequency.
- Droplet roll-off characteristics can be strongly altered by electrowetting fields, It is possible to control the roll-off size and frequency via selection of the applied waveform.
- Condensate removal depends on the size and frequency of droplets rolling off, and on the amount of liquid captured by the droplets as they roll off.
- Condensation rate can be increased by over 30% by applying AC electric fields.

Findings from this study can be the basis for developing technologies to enhance condensation rates for various applications. This work also identifies additional strategies, which can be used to enhance droplet coalescence such as

selection of appropriate waveforms and periodic use of electrowetting fields. The use of electrowetting coupled with surface engineering offers opportunities for even higher enhancements in condensation heat transfer via the control of phenomena which influence droplet coalescence and roll-off.

Acknowledgements

References

[1] Wikramanayake, E. D., Ozkan, O., and Bahadur, V., 2017, "Landfill Gas-Powered Atmospheric Water Harvesting (AWH) for Oilfield Operations in the United States," Energy, **138**, pp. 647–658.

[2] Paxson, A. T., Yagüe, J. L., Gleason, K. K., and Varanasi, K. K., 2014, "Stable Dropwise Condensation for Enhancing Heat Transfer via the Initiated Chemical Vapor Deposition (ICVD) of Grafted Polymer Films," Adv. Mater., **26**(3), pp. 418–423.

[3] Reifert, V. G., Sardak, A. I., Grigorenko, S. V., and Podbereznyj, V. L., 1989, "Heat Exchange at Dropwise Condensation in Heat Exchangers of Desalination Plants," Desalination, **74**, pp. 373–382.

[4] Rose, J. W., 2002, "Dropwise Condensation Theory and Experiment: A Review," Proc. Inst. Mech. Eng. Part A J. Power Energy, **216**(2), pp. 115–128.

[5] Miljkovic, N., Enright, R., and Wang, E. N., 2013, "Modeling and Optimization of Superhydrophobic Condensation," J. Heat Transfer, **135**(11), p. 111004.

[6] Azar, A., Bahadur, V., Kulkarni, A., Yamada, M., and Ruud, J. A., 2013, "Hydrophobic Surfaces for Control and Enhancement of Water Phase Transitions," MRS Bull. Interfacial Mater. with Spec. Wettability, **38**(5), pp. 407–411.

[7] Weisensee, P. B., Wang, Y., Hongliang, Q., Schultz, D., King, W. P., and Miljkovic, N., 2017, "Condensate Droplet Size Distribution on Lubricant-Infused Surfaces," Int. J. Heat Mass Transf., **109**, pp. 187–199.

[8] Mondal, B., Mac Giolla Eain, M., Xu, Q. F., Egan, V. M., Punch, J., and Lyons, A. M., 2015, "Design and Fabrication of a Hybrid Superhydrophobic-Hydrophilic Surface That Exhibits Stable Dropwise Condensation," ACS Appl. Mater. Interfaces, **7**(42), pp. 23575–23588.

[9] Chu, F., Wu, X., and Ma, Q., 2017, "Condensed Droplet Growth on Surfaces with Various Wettability," **115**, pp. 1101–1108.

[10] Zhao, Y., Preston, D. J., Lu, Z., Zhang, L., Queeney, J., and Wang, E. N., 2018, "Effects of Millimetric Geometric Features on Dropwise Condensation under Different Vapor Conditions," Int. J. Heat Mass Transf., **119**, pp. 931–938.

[11] Miljkovic, N., Enright, R., and Wang, E. N., 2012, "Growth Dynamics During Dropwise Condensation On," *ASME 2012 3rd Micro/Nanoscale Heat & Mass Transfer International Conference MNHMT2012*, pp. 1–10.

[12] Kim, S., and Kim, K. J., 2011, "Dropwise Condensation Modeling Suitable for Superhydrophobic Surfaces," J. Heat Transfer, **133**(8), p. 081502.

[13] Dey, R., Gilbers, J., Baratian, D., Hoek, H., van den Ende, D., and Mugele, F., 2018, "Controlling Shedding Characteristics of Condensate Drops Using Electrowetting," Appl. Phys. Lett., **113**.

[14] Baratian, D., Dey, R., Hoek, H., Van Den Ende, D., and Mugele, F., 2018, "Breath Figures under Electrowetting: Electrically Controlled Evolution of Drop Condensation Patterns," Phys. Rev. Lett., **120**(21), p. 214502.

[15] Mugele, F., and Baret, J.-C., 2005, "Electrowetting: From Basics to Applications," J. Phys. Condens. Matter, **17**(28), pp. R705–R774.

[16] Chen, L., and Bonaccurso, E., 2014, "Electrowetting — From Statics to Dynamics," Adv. Colloid Interface Sci., **210**, pp. 2–12.

[17] Chen, J. Z., Darhuber, A. A., Troian, S. M., and Wagner, S., 2004, "Capacitive Sensing of Droplets for Microfluidic Devices Based on Thermocapillary Actuation," Lab Chip, **4**(5), pp. 473–480.

[18] Elbuken, C., Glawdel, T., Chan, D., and Ren, C. L., 2011, "Detection of Microdroplet Size and Speed Using Capacitive Sensors," Sensors Actuators, A Phys., **171**(2), pp. 55–62.

[19] Kumari, N., Bahadur, V., and Garimella, S. V., 2008, "Electrical Actuation of Electrically Conducting and Insulating Droplets Using Ac and Dc Voltages," J. Micromechanics Microengineering, **18**(10).

[20] Wikramanayake, E. D., and Bahadur, V., 2019, "Electrowetting-Based Enhancement of Droplet Growth Dynamics and Heat Transfer during Humid Air Condensation," Int. J. Heat Mass Transf., **140**, pp. 260–268.

[21] Castillo, J. E., Weibel, J. a., and Garimella, S. V., 2015, "The Effect of Relative Humidity on Dropwise Condensation Dynamics," Int. J. Heat Mass Transf., **80**, pp. 759–766.

[22] Leach, R. N., Stevens, F., Langford, S. C., and Dickinson, J. T., 2006, "Dropwise Condensation: Experiments and Simulations of Nucleation and Growth of Water Drops in a Cooling System.," Langmuir, **22**(3), pp. 8864–8872.

[23] Watanabe, N., Aritomi, M., and Machida, A., 2014, "Time-Series Characteristics and Geometric Structures of Drop-Size Distribution Density in Dropwise Condensation," Int. J. Heat Mass Transf., **76**, pp. 467–483.